Processing and visualization for diffusion tensor MRI

C.-F. Westin*, S.E. Maier, H. Mamata, A. Nabavi, F.A. Jolesz, R. Kikinis

Brigham & Women's Hospital, Harvard Medical School, Department of Radiology, 75 Francis Street, Boston, MA 02115, USA

Abstract

This paper presents processing and visualization techniques for Diffusion Tensor Magnetic Resonance Imaging (DT-MRI). In DT-MRI, each voxel is assigned a tensor that describes local water diffusion. The geometric nature of diffusion tensors enables us to quantitatively characterize the local structure in tissues such as bone, muscle, and white matter of the brain. This makes DT-MRI an interesting modality for image analysis. In this paper we present a novel analytical solution to the Stejskal–Tanner diffusion equation system whereby a dual tensor basis, derived from the diffusion sensitizing gradient configuration, eliminates the need to solve this equation for each voxel. We further describe decomposition of the diffusion tensor based on its symmetrical properties, which in turn describe the geometry of the diffusion ellipsoid. A simple anisotropy measure follows naturally from this analysis. We describe how the geometry or shape of the tensor can be visualized using a coloring scheme based on the derived shape measures. In addition, we demonstrate that human brain tensor data when filtered can effectively describe macrostructural diffusion, which is important in the assessment of fiber-tract organization. We also describe how white matter pathways can be monitored with the methods introduced in this paper. DT-MRI tractography is useful for demonstrating neural connectivity (in vivo) in healthy and diseased brain tissue. © 2002 Elsevier Science B.V. All rights reserved.

Keywords: Diffusion Tensor MRI; Tractography; Dual basis; Geometrical diffusion measures; Visualization

1. Introduction

Diffusion is the process by which matter is transported from one part of a system to another owing to random molecular motions. The transfer of heat by conduction is also due to random molecular motion. The analogous nature of the two processes was first recognized by Fick (1855), who described diffusion quantitatively by adopting the mathematical equation of heat conduction derived some years earlier by Fourier (1822). Fick's law states that local differences in solute concentration will give rise to a net flux of solute molecules from high concentration regions to low concentration regions. The net amount of material diffusing across a unit cross-section that is perpendicular to a direction is proportional to the concentration gradient. Thus, the phenomenon of diffusion was described scientifically before any systematic development of thermodynamics. This phenomenon, known as Brownian Motion, is named after the botanist, Robert Brown, who observed the movement of plant spores floating in water in 1827. The first satisfactory theoretical treatment of Brownian Motion, however, was not made until much later by Albert Einstein (1905) and provided strong circumstantial evidence for the existence of molecules.

Anisotropic media such as crystals, textile fibers, and polymer films have different diffusion properties depending on direction. Anisotropic diffusion is best described by an ellipsoid where the radius defines the diffusion in a particular direction. The widely accepted analogy between symmetric 3×3 tensors and ellipsoids makes such tensors natural descriptors for diffusion. Moreover, the geometric nature of the diffusion tensors can quantitatively characterize the local structure in tissues such as bone, muscle, and

*Corresponding author. Tel.: +1-617-278-0986; fax: +1-617-582-6033.

E-mail address: westin@bwh.harvard.edu (C.-F. Westin).

white matter of the brain. Within white matter, the mobility of the water is restricted by the axons that are oriented along the fiber tracts. This anisotropic diffusion is due to tightly packed multiple myelin membranes encompassing the axon. Although myelination is not essential for diffusion anisotropy of nerves [as shown in studies of non-myelinated garfish olfactory nerves (Beaulieu and Allen, 1994); and in studies where anisotropy exists in brains of neonates before the histological appearance of myelin (Wimberger et al., 1995)], myelin is generally assumed to be the major barrier to diffusion in myelinated fiber tracts.

Using conventional MRI, we can easily identify the functional centers of the brain (cortex and nuclei). However, with conventional proton magnetic resonance imaging (MRI) techniques, the white matter of the brain appears to be homogeneous without any suggestion of the complex arrangement of fiber tracts. Hence, the demonstration of anisotropic diffusion in the brain by magnetic resonance has paved the way for non-invasive exploration of the structural anatomy of the white matter in vivo (Moseley et al., 1990; Chenevert et al., 1990; Basser, 1995; Pierpaoli et al., 1996).

The paper is organized as follows. First, we review the basics of DT-MRI (Section 2). Section 3.1 presents a new method for calculating the diffusion tensors from the diffusion gradient raw data. The method is based on an analytic solution of the Stejskal–Tanner formula eliminating the need to solve the Stejskal–Tanner equation system for each voxel of the data set. In Section 4, we expand on our previous quantitative characterization of the geometric nature of the diffusion tensors (Westin et al., 1997, 1999) by capturing macrostructural diffusion properties, and depicting detailed in vivo images of human white matter tracts. Using these methods, we can identify the orientation and distribution of most of the known major fiber tracts. In Section 5, we discuss visualization methods for tensor diffusion data and describe a method relating to the barycentric tensor shape descriptors from Section 4. We conclude by describing a novel white matter tractography method (expanded from Westin et al., 1999) and show some tractography results from axial DT-MRI data of the brain (Section 6).

2. Diffusion tensor MRI

DT-MRI is a relatively recent MR imaging modality used for relating image intensities to the relative mobility of endogenous tissue water molecules. In DT-MRI, a tensor describing local water diffusion is calculated for each voxel from measurements of diffusion in several directions. To measure diffusion, the Stejskal–Tanner imaging sequence is used (Stejskal and Tanner, 1965). This sequence uses two strong gradient pulses, symmetrically positioned around a 180° refocusing pulse, allowing for controlled diffusion weighting (Fig. 1). The first gradient pulse induces a phase shift for all spins; the second gradient pulse will invert this phase shift, thus canceling the phase shift for static spins. Spins having completed a change of location due to Brownian Motion during the time period (Δ in Fig. 1) will experience different phase shifts by the two gradient pulses, which means they are not completely refocused and consequently will result in a signal loss.

To eliminate the dependence of spin density, T1, and T2 we must take at least two measurements of diffusion-weighted images that are differently sensitized to diffusion but remain identical in all other respects. By using, for instance, a measurement *without* diffusion weighting and one *with* diffusion weighting, diffusion can be calculated using the following equation (Stejskal and Tanner, 1965):

$$S = S_0 \, e^{-bD}, \tag{1}$$

where b is the diffusion weighting factor, introduced and defined by LeBihan et al. (1986),

$$b = \gamma^2 \delta^2 \left(\Delta - \frac{\delta}{3} \right) |\mathbf{g}|^2, \tag{2}$$

where γ is the proton gyromagnetic ratio (42 MHz/Tesla), $|\mathbf{g}|$ is the strength of the diffusion sensitizing gradient pulses, δ is the duration of the diffusion gradient pulses, and Δ is the time between diffusion gradient RF pulses (Fig. 1). The diffusion values, D, are also known as 'apparent diffusion components' (or ADC values), which emphasizes the fact that the diffusion values generated from this procedure depend on the experimental conditions

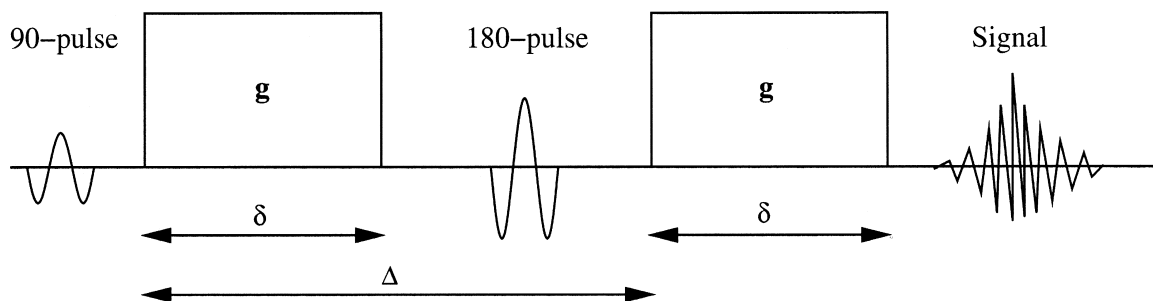
Fig. 1. The Stejskal–Tanner imaging sequence.

such as the direction of the sensitizing gradient and other sequence parameters (δ and Δ).

2.1. Imaging parameters

In this work we applied a version of the Line Scan Diffusion Imaging (LSDI) technique (Gudbjartsson et al., 1996; Maier and Gudbjartsson, 1998; Maier et al., 1998). This method, like the commonly used diffusion-sensitized, ultrafast, echo-planar imaging (EPI) technique (Turner et al., 1990), is relatively insensitive to bulk motion and physiologic pulsations of vascular origin.

Our data were acquired at the Brigham and Women's Hospital on a GE Signa 1.5 Tesla Horizon Echospeed 5.6 system with standard 2.2 Gauss/cm field gradients. The time required for acquisition of the diffusion tensor data for one slice was 1 min; no averaging was performed. Imaging parameters were: effective TR = 2.4 s, TE = 65 ms, $b_{high} = 1000$ s/mm^2, $b_{low} = 5$ s/mm^2, field of view 22 cm, effective voxel size $4.0 \times 1.7 \times 1.7$ mm^3, 4 kHz readout bandwidth, acquisition matrix 128×128.

2.2. Calculation of diffusion tensors

For the case of anisotropic diffusion, Eq. (1) has to be written in a more general form,

$$S = S_0\, e^{-\gamma^2 \delta^2 [\Delta - (\delta/3)] \mathbf{g}^T \mathbf{D} \mathbf{g}}. \tag{3}$$

This formula reverts to the isotropic case above with $\mathbf{D} = D\mathbf{I}$, where $\mathbf{I}$ is the identity tensor. By inserting normalized gradient vectors, $\hat{\mathbf{g}} = \mathbf{g}/|\mathbf{g}|$, we can then write Eq. (3) using LeBihan's b-factor (Eq. (2)),

$$S = S_0\, e^{-b \hat{\mathbf{g}}^T \mathbf{D} \hat{\mathbf{g}}}. \tag{4}$$

In the typical case, the symmetric 3×3 diffusion tensor $\mathbf{D}$ has six degrees of freedom (number of independent coefficients in a matrix representation). To estimate the tensor, then, at least six measurements (taken from different non-collinear gradient directions) are needed, in addi-

tion to the baseline image data S_0. Thus for each slice in the data set, seven images need to be collected with different diffusion weightings and gradient directions. Fig. 2 shows an example of such data with corresponding gradient directions, where $\{S_0, S_1, \ldots, S_6\}$ represent the signal intensities in the presence of gradients $\mathbf{g}_k$. S_0 is the signal intensity in the absence of a diffusion-sensitizing field gradient ($|\mathbf{g}_0| = 0$), giving the baseline to which the remaining measurements can be related. Inserting the gradients $\mathbf{g}_k$ and the signals $\{S_k\}$ into the equation for the loss in signal intensity (Eq. (3)) results in

$$S_k = S_0\, e^{-b \hat{\mathbf{g}}_k^T \mathbf{D} \hat{\mathbf{g}}_k}, \tag{5}$$

a system of six equations from which the tensor can be calculated,

$$\begin{cases}
\ln(S_1) = \ln(S_0) - b\hat{\mathbf{g}}_1^T \mathbf{D} \hat{\mathbf{g}}_1, \\
\ln(S_2) = \ln(S_0) - b\hat{\mathbf{g}}_2^T \mathbf{D} \hat{\mathbf{g}}_2, \\
\ln(S_3) = \ln(S_0) - b\hat{\mathbf{g}}_3^T \mathbf{D} \hat{\mathbf{g}}_3, \\
\ln(S_4) = \ln(S_0) - b\hat{\mathbf{g}}_4^T \mathbf{D} \hat{\mathbf{g}}_4, \\
\ln(S_5) = \ln(S_0) - b\hat{\mathbf{g}}_5^T \mathbf{D} \hat{\mathbf{g}}_5, \\
\ln(S_6) = \ln(S_0) - b\hat{\mathbf{g}}_6^T \mathbf{D} \hat{\mathbf{g}}_6.
\end{cases} \tag{6}$$

By solving this equation system for each voxel in the data set, we will arrive at the final diffusion tensor field.

3. Tensor form of Stejskal–Tanner equations

3.1. Dual bases and diffusion measurements

In this section we will derive a compact analytic solution to the Stejskal–Tanner equation system (Eq. (6)) using concepts from tensor analysis. Tensor analysis is a multi-linear extension of traditional linear algebra and a generalization of the notions from vector analysis. Central concepts in tensor analysis are dual spaces and con-

$$\mathbf{g}_0 = \begin{pmatrix} 0 \\ 0 \\ 0 \end{pmatrix} \quad \mathbf{g}_1 = \begin{pmatrix} 1 \\ 1 \\ 0 \end{pmatrix} \quad \mathbf{g}_2 = \begin{pmatrix} 0 \\ 1 \\ 1 \end{pmatrix} \quad \mathbf{g}_3 = \begin{pmatrix} 1 \\ 0 \\ 1 \end{pmatrix} \quad \mathbf{g}_4 = \begin{pmatrix} 0 \\ 1 \\ -1 \end{pmatrix} \quad \mathbf{g}_5 = \begin{pmatrix} 1 \\ -1 \\ 0 \end{pmatrix} \quad \mathbf{g}_6 = \begin{pmatrix} -1 \\ 0 \\ 1 \end{pmatrix}$$
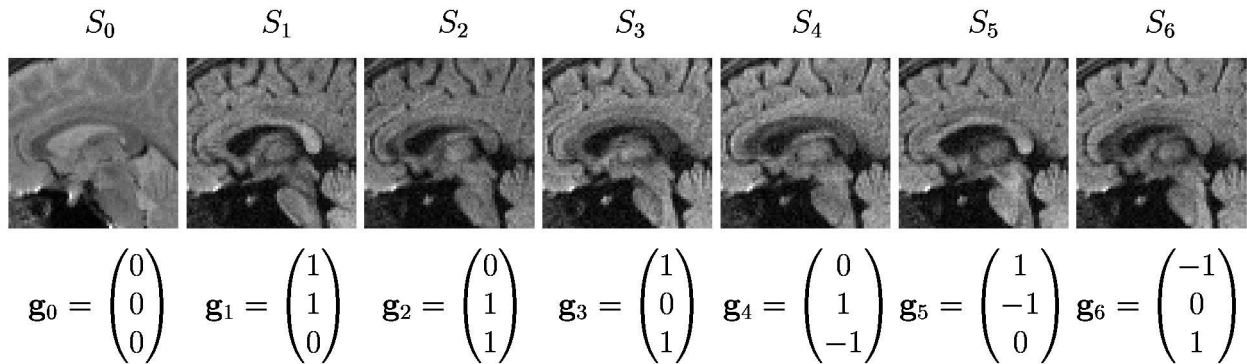
Fig. 2. Examples of sagittal diffusion measurements with corresponding magnetic field gradients used for diffusion weighting.

travariant vectors. Details on this topic can be found in textbooks on vector analysis and differential geometry, including (Stoker, 1989; Young, 1978; Kendall, 1977).

Tensor algebra states that for finite dimensional spaces every element can decomposed on a basis

$$\mathbf{D} = \sum_k \alpha_k \mathbf{G}_k, \tag{7}$$

where α_k are the coordinates of $\mathbf{D}$ in the basis $\mathbf{G}_k$. If the basis is orthonormal, the coordinates α_k are the inner products of the element with the basis elements. If the basis is not orthonormal, the α_k are the inner products of the element with the dual basis elements, here denoted $\tilde{\mathbf{G}}_k$. To be more precise, the coordinates are always the inner products of the element with the dual basis elements, however for an orthonormal basis, the dual basis coincides with the original basis: $\tilde{\mathbf{G}}_k = \mathbf{G}_k$

$$\mathbf{D} = \sum_k \langle \tilde{\mathbf{G}}_k, \mathbf{D} \rangle \mathbf{G}_k. \tag{8}$$

The elements can also be expressed in the dual basis, and by symmetry the coordinates are obtained by projecting onto the dual of the dual basis, which is the original basis itself,

$$\mathbf{D} = \sum_k \langle \mathbf{G}_k, \mathbf{D} \rangle \tilde{\mathbf{G}}_k. \tag{9}$$

Fig. 3 shows an example of how to graphically construct a dual basis from a basis by drawing parallel lines along the vectors and lines touching the end of the vectors. From the figure, it can be seen that if the original basis were orthonormal, the dual basis vectors and the basis vectors would coincide, and the difference between the basis sets would become more of a theoretical issue rather than a

practical one. As evidenced below, the diffusion basis functions arising from MR scanner measurements are non-orthogonal; thus its dual elements have practical implications. Diffusion tensors belong to the class of symmetric 3×3 tensors and have six degrees of freedom, meaning that six different basis tensors are required to span this space. Thus we may write

$$\mathbf{D} = \sum_{k=1}^{6} \langle \tilde{\mathbf{G}}_k, \mathbf{D} \rangle \mathbf{G}_k, \tag{10}$$

where the weights α_k are the coordinates of $\mathbf{D}$ in the (tensor) basis $\{\mathbf{G}_1, \mathbf{G}_2, \ldots, \mathbf{G}_6\}$.

Reverting to the Stejskal–Tanner equation (Eq. (3)), and noting that the double projection of the gradient vectors can be rewritten using an inner product (contraction) between the diffusion tensor and the outer product of the gradient directions,

$$\hat{\mathbf{g}}^{\mathrm{T}} \mathbf{D} \hat{\mathbf{g}} = \langle \mathbf{G}, \mathbf{D} \rangle, \tag{11}$$

where

$$\mathbf{G} = \hat{\mathbf{g}} \hat{\mathbf{g}}^{\mathrm{T}}, \tag{12}$$

and inserting this result gives the following expression of the Stejskal–Tanner equations:

$$\ln(S_k) = \ln(S_0) - b \langle \mathbf{G}_k, \mathbf{D} \rangle, \tag{13}$$

which give closed expressions for the inner products,

$$\langle \mathbf{G}_k, \mathbf{D} \rangle = \frac{1}{b} (\ln(S_0) - \ln(S_k)). \tag{14}$$

Recalling the structure of the coordinates and basis elements for the diffusion tensor in Eq. (9) we see that Eq. (14) describes the dual coordinates of the diffusion tensor
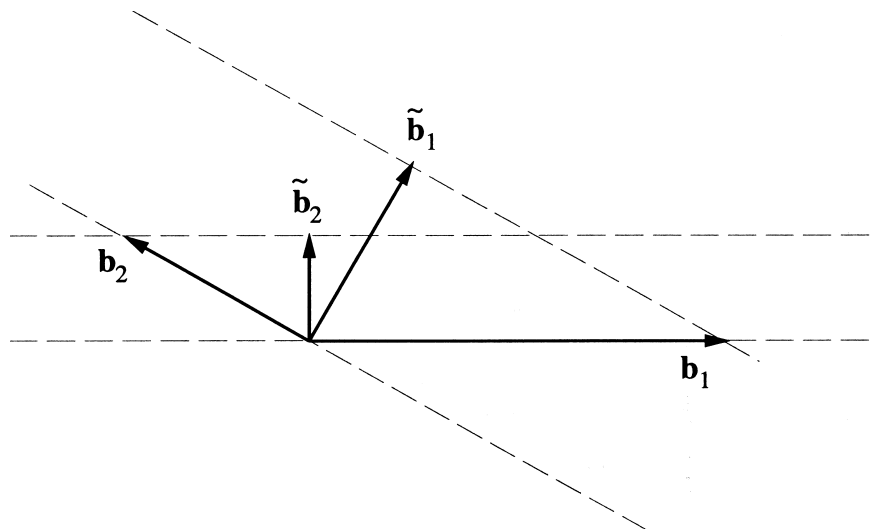

Fig. 3. Graphical construction of a dual basis in 2D. Two lines are drawn along the basis vectors $\mathbf{b}_1$ and $\mathbf{b}_2$, and two lines are drawn parallel to these touching the end of the vectors. The parallel lines represent a dual basis, which also can be graphically illustrated in a vector form: two vectors that are perpendicular to the lines, $\tilde{\mathbf{b}}_1$ and $\tilde{\mathbf{b}}_2$.

expressed by the diffusion data from the scanner S_k and the b-factor. By identifying the dual basis to $\mathbf{G}$, the outer product of the gradient directions, Eq. (9) gives that the diffusion tensor can be directly calculated by a simple linear sum,

$$\mathbf{D} = \sum_{k=1}^{6} \frac{1}{b}(\ln(S_0) - \ln(S_k))\tilde{\mathbf{G}}_k. \qquad (15)$$

The set of six outer product gradient tensors $\{\mathbf{G}_k\}$, $k \in 1, \dots, 6$, defines a (non-orthogonal) tensor basis and the corresponding dual tensor basis $\{\tilde{\mathbf{G}}_k\}$ is uniquely defined by the following bi-orthogonal relation:

$$\langle \mathbf{G}_i, \tilde{\mathbf{G}}_k \rangle = \delta_{ik}, \qquad (16)$$

where Kronecker's symbol δ_{ij} is used with the usual meaning, $\delta = 1$ if $i = j$ and 0 if $i \neq j$. See, for example, (Westin, 1994) for more details about non-orthogonal bases.

3.2. Calculation of dual tensor basis

In this section we will derive the dual tensor basis corresponding to the specific gradient configuration in our DT-MRI protocol. The gradient directions used in our experiments are

$$\mathbf{g}_1 = \frac{1}{\sqrt{2}}\begin{pmatrix} 1 \\ 1 \\ 0 \end{pmatrix}, \qquad \mathbf{g}_2 = \frac{1}{\sqrt{2}}\begin{pmatrix} 0 \\ 1 \\ 1 \end{pmatrix}, \qquad \mathbf{g}_3 = \frac{1}{\sqrt{2}}\begin{pmatrix} 1 \\ 0 \\ 1 \end{pmatrix},$$

$$\mathbf{g}_4 = \frac{1}{\sqrt{2}}\begin{pmatrix} 0 \\ 1 \\ -1 \end{pmatrix}, \qquad \mathbf{g}_5 = \frac{1}{\sqrt{2}}\begin{pmatrix} 1 \\ -1 \\ 0 \end{pmatrix}, \qquad \mathbf{g}_6 = \frac{1}{\sqrt{2}}\begin{pmatrix} -1 \\ 0 \\ 1 \end{pmatrix}, \qquad (17)$$

giving the following outer products of these gradients:

$$\mathbf{G}_1 = \frac{1}{2}\begin{pmatrix} 1 & 1 & 0 \\ 1 & 1 & 0 \\ 0 & 0 & 0 \end{pmatrix}, \qquad \mathbf{G}_2 = \frac{1}{2}\begin{pmatrix} 0 & 0 & 0 \\ 0 & 1 & 1 \\ 0 & 1 & 1 \end{pmatrix},$$

$$\mathbf{G}_3 = \frac{1}{2}\begin{pmatrix} 1 & 0 & 1 \\ 0 & 0 & 0 \\ 1 & 0 & 1 \end{pmatrix}, \qquad (18)$$

$$\mathbf{G}_4 = \frac{1}{2}\begin{pmatrix} 0 & 0 & 0 \\ 0 & 1 & -1 \\ 0 & -1 & 1 \end{pmatrix}, \qquad \mathbf{G}_5 = \frac{1}{2}\begin{pmatrix} 1 & -1 & 0 \\ -1 & 1 & 0 \\ 0 & 0 & 0 \end{pmatrix},$$

$$\mathbf{G}_6 = \frac{1}{2}\begin{pmatrix} 1 & 0 & -1 \\ 0 & 0 & 0 \\ -1 & 0 & 1 \end{pmatrix}. \qquad (19)$$

A convenient way of finding the dual basis to $\mathbf{G}_k$ is by stacking the coordinates of each tensor basis element as column vectors in a matrix, and calculating the pseudo inverse of this matrix $\tilde{\mathbf{G}} = \mathbf{G}^{\dagger}$,

$$\begin{pmatrix} | & | & \cdots & | \\ \mathbf{G}_1 & \mathbf{G}_2 & \cdots & \mathbf{G}_6 \\ | & | & \cdots & | \end{pmatrix}^{\dagger}$$

$$= \left(\frac{1}{2}\begin{pmatrix} 1 & 0 & 1 & 0 & 1 & 1 \\ 1 & 0 & 0 & 0 & -1 & 0 \\ 0 & 0 & 1 & 0 & 0 & -1 \\ 1 & 0 & 0 & 0 & -1 & 0 \\ 1 & 1 & 0 & 1 & 1 & 0 \\ 0 & 1 & 0 & -1 & 0 & 0 \\ 0 & 0 & 1 & 0 & 0 & -1 \\ 0 & 1 & 0 & -1 & 0 & 0 \\ 0 & 1 & 1 & 1 & 0 & 1 \end{pmatrix} \right)^{\dagger} \qquad (20)$$

$$= \frac{1}{2}\begin{pmatrix} 1 & 1 & 0 & 1 & 1 & 0 & 0 & 0 & -1 \\ -1 & 0 & 0 & 0 & 1 & 1 & 0 & 1 & 1 \\ 1 & 0 & 1 & 0 & -1 & 0 & 1 & 0 & 1 \\ -1 & 0 & 0 & 0 & 1 & -1 & 0 & -1 & 1 \\ 1 & -1 & 0 & -1 & 1 & 0 & 0 & 0 & -1 \\ 1 & 0 & -1 & 0 & -1 & 0 & -1 & 0 & 1 \end{pmatrix}. \qquad (21)$$

Inserting this result verifies the bi-orthonormality requirement between the basis and dual basis elements:

$$\tilde{\mathbf{G}}\mathbf{G} = \begin{pmatrix} | & | & \cdots & | \\ \tilde{\mathbf{G}}_1 & \tilde{\mathbf{G}}_2 & \cdots & \tilde{\mathbf{G}}_6 \\ | & | & \cdots & | \end{pmatrix}^{\mathrm{T}} \begin{pmatrix} | & | & \cdots & | \\ \mathbf{G}_1 & \mathbf{G}_2 & \cdots & \mathbf{G}_6 \\ | & | & \cdots & | \end{pmatrix} \qquad (22)$$

$$= \underbrace{\frac{1}{2}\begin{pmatrix} 1 & 1 & 0 & 1 & 1 & 0 & 0 & 0 & -1 \\ -1 & 0 & 0 & 0 & 1 & 1 & 0 & 1 & 1 \\ 1 & 0 & 1 & 0 & -1 & 0 & 1 & 0 & 1 \\ -1 & 0 & 0 & 0 & 1 & -1 & 0 & -1 & 1 \\ 1 & -1 & 0 & -1 & 1 & 0 & 0 & 0 & -1 \\ 1 & 0 & -1 & 0 & -1 & 0 & -1 & 0 & 1 \end{pmatrix}}_{\text{dual basis}}$$

$$\times \underbrace{\frac{1}{2}\begin{pmatrix} 1 & 0 & 1 & 0 & 1 & 1 \\ 1 & 0 & 0 & 0 & -1 & 0 \\ 0 & 0 & 1 & 0 & 0 & -1 \\ 1 & 0 & 0 & 0 & -1 & 0 \\ 1 & 1 & 0 & 1 & 1 & 0 \\ 0 & 1 & 0 & -1 & 0 & 0 \\ 0 & 0 & 1 & 0 & 0 & -1 \\ 0 & 1 & 0 & -1 & 0 & 0 \\ 0 & 1 & 1 & 1 & 0 & 1 \end{pmatrix}}_{\text{basis}} \qquad (23)$$

$$= \begin{pmatrix} 1 & 0 & 0 & 0 & 0 & 0 \\ 0 & 1 & 0 & 0 & 0 & 0 \\ 0 & 0 & 1 & 0 & 0 & 0 \\ 0 & 0 & 0 & 1 & 0 & 0 \\ 0 & 0 & 0 & 0 & 1 & 0 \\ 0 & 0 & 0 & 0 & 0 & 1 \end{pmatrix} = \mathbf{I}. \qquad (24)$$

The rows of the pseudo inverse (Eq. (21)) contain the dual basis elements. Reshaping them into 3×3 tensors gives

$$\tilde{\mathbf{G}}_1 = \frac{1}{2}\begin{pmatrix} 1 & 1 & 0 \\ 1 & 1 & 0 \\ 0 & 0 & -1 \end{pmatrix}, \quad \tilde{\mathbf{G}}_2 = \frac{1}{2}\begin{pmatrix} -1 & 0 & 0 \\ 0 & 1 & 1 \\ 0 & 1 & 1 \end{pmatrix},$$

$$\tilde{\mathbf{G}}_3 = \frac{1}{2}\begin{pmatrix} 1 & 0 & 1 \\ 0 & -1 & 0 \\ 1 & 0 & 1 \end{pmatrix}, \quad \tilde{\mathbf{G}}_4 = \frac{1}{2}\begin{pmatrix} -1 & 0 & 0 \\ 0 & 1 & -1 \\ 0 & -1 & 1 \end{pmatrix}$$

$$\tilde{\mathbf{G}}_5 = \frac{1}{2}\begin{pmatrix} 1 & -1 & 0 \\ -1 & 1 & 0 \\ 0 & 0 & -1 \end{pmatrix}, \quad \tilde{\mathbf{G}}_6 = \frac{1}{2}\begin{pmatrix} 1 & 0 & -1 \\ 0 & -1 & 0 \\ -1 & 0 & 1 \end{pmatrix}.$$

Since the dual tensor basis is defined solely by the gradient configuration and is not dependent on the data, the diffusion tensors can be described by a linear sum of constant tensor elements,

$$\mathbf{D} = \sum_{k=1}^{6} \beta_k \tilde{\mathbf{G}}_k, \tag{25}$$

where the dual coordinates are (Eq. (14))

$$\beta_k = \frac{1}{b}(\ln(S_0) - \ln(S_i)). \tag{26}$$

The presented method gives an analytical solution to the Steskal–Tanner equation system, and eliminates the need to solve this equation system for every data point.

In Appendix A, the dual tensor basis corresponding to the gradient configuration in (Basser and Pierpaoli, 1996) is calculated as an additional example of how the method works.

4. Anisotropy and macrostructural measures

Since MRI methods, in general, obtain a macroscopic measure of a microscopic quantity (which necessarily entails intravoxel averaging), the voxel dimensions influence the measured diffusion tensor at any given location in the brain. Factors affecting the shape of the apparent diffusion tensor (shape of the diffusion ellipsoid) in the white matter include the density of fibers, the degree of myelination, the average fiber diameter and the directional similarity of the fibers in the voxel. The geometric nature of the measured diffusion tensor within a voxel is thus a meaningful measure of fiber tract organization. The advent of robust diffusion tensor imaging techniques has prompted the development of quantitative measures for describing the diffusion anisotropy. However, to relate the measure of diffusion anisotropy to the structural geometry of the tissue, a mathematical description of diffusion tensors and their quantification is necessary (Basser, 1995). Several different measures of anisotropy have been proposed in the literature. Among the most popular are two that are based on the normalized variance of the eigenvalues; the relative anisotropy (RA) and the fractional anisotropy (FA) (Basser and Pierpaoli, 1996). An advantage of these measures is that they can be calculated without first explicitly calculating any eigenvalues. Both anisotropy measures can be expressed in terms of the norm and the trace of the diffusion tensor (the norm is calculated as the square root of the sum of the squared elements of the tensor which equals the square root of the sum of the squared eigenvalues, and the trace is calculated as the sum of the diagonal elements which equals the sum of the eigenvalues),

$$RA = \frac{1}{\sqrt{2}} \frac{\sqrt{(\lambda_1 - \lambda_2)^2 + (\lambda_2 - \lambda_3)^2 + (\lambda_1 - \lambda_3)^2}}{(\lambda_1 + \lambda_2 + \lambda_3)}$$

$$= \frac{\sqrt{3}}{\sqrt{2}} \frac{|\mathbf{D} - \frac{1}{3}\mathrm{trace}(\mathbf{D})\mathbf{I}|}{\mathrm{trace}(\mathbf{D})}, \tag{27}$$

$$FA = \frac{1}{\sqrt{2}} \frac{\sqrt{(\lambda_1 - \lambda_2)^2 + (\lambda_2 - \lambda_3)^2 + (\lambda_1 - \lambda_3)^2}}{\sqrt{\lambda_1^2 + \lambda_2^2 + \lambda_3^2}}$$

$$= \frac{\sqrt{3}}{\sqrt{2}} \frac{|\mathbf{D} - \frac{1}{3}\mathrm{trace}(\mathbf{D})\mathbf{I}|}{|\mathbf{D}|}, \tag{28}$$

where $\mathbf{I}$ is the identity tensor. The constants are inserted to ensure that the measures are in the range from zero to one. In the next section we will present alternatives to these measures based on the geometric properties of the diffusion ellipsoid.

4.1. Geometrical measures of diffusion

The diffusion tensor can be visualized using an ellipsoid where the principal axes correspond to the directions of the eigenvector system. Using symmetry properties of this ellipsoid, the diffusion tensor can be decomposed into basic geometric measures (Westin et al., 1997), a concept upon which we will elaborate in this section.

Let $\lambda_1 \geq \lambda_2 \geq \lambda_3 \geq 0$ be the eigenvalues of the symmetric diffusion tensor $\mathbf{D}$, and let $\hat{\mathbf{e}}_i$ be the normalized eigenvector corresponding to λ_i. The tensor $\mathbf{D}$ can then be described by

$$\mathbf{D} = \lambda_1 \hat{\mathbf{e}}_1 \hat{\mathbf{e}}_1^{\mathrm{T}} + \lambda_2 \hat{\mathbf{e}}_2 \hat{\mathbf{e}}_2^{\mathrm{T}} + \lambda_3 \hat{\mathbf{e}}_3 \hat{\mathbf{e}}_3^{\mathrm{T}}. \tag{29}$$

Diffusion can be divided into three basic cases depending on the rank of the diffusion tensor,
- Linear case ($\lambda_1 \gg \lambda_2 \simeq \lambda_3$): diffusion is mainly in the direction corresponding to the largest eigenvalue,

$$\mathbf{D} \simeq \lambda_1 \mathbf{D}_l = \lambda_1 \hat{\mathbf{e}}_1 \hat{\mathbf{e}}_1^{\mathrm{T}}. \tag{30}$$

- Planar case ($\lambda_1 \simeq \lambda_2 \gg \lambda_3$): diffusion is restricted to a plane spanned by the two eigenvectors corresponding to the two largest eigenvalues,

$$\mathbf{D} \simeq \lambda_1 \mathbf{D}_p = \lambda_1 (\hat{\mathbf{e}}_1 \hat{\mathbf{e}}_1^{\mathrm{T}} + \hat{\mathbf{e}}_2 \hat{\mathbf{e}}_2^{\mathrm{T}}). \tag{31}$$

- Spherical case ($\lambda_1 \simeq \lambda_2 \simeq \lambda_3$): isotropic diffusion,

$$\mathbf{D} \simeq \lambda_1 \mathbf{D}_s = \lambda_1 (\hat{\mathbf{e}}_1 \hat{\mathbf{e}}_1^{\mathrm{T}} + \hat{\mathbf{e}}_2 \hat{\mathbf{e}}_2^{\mathrm{T}} + \hat{\mathbf{e}}_3 \hat{\mathbf{e}}_3^{\mathrm{T}}). \tag{32}$$

In general, the diffusion tensor $\mathbf{D}$ will be a combination of these cases. Expanding the diffusion tensor using these cases as a basis gives

$$\begin{aligned}\mathbf{D} &= \lambda_1 \hat{\mathbf{e}}_1 \hat{\mathbf{e}}_1^T + \lambda_2 \hat{\mathbf{e}}_2 \hat{\mathbf{e}}_2^T + \lambda_3 \hat{\mathbf{e}}_3 \hat{\mathbf{e}}_3^T \\ &= (\lambda_1 - \lambda_2)\hat{\mathbf{e}}_1 \hat{\mathbf{e}}_1^T + (\lambda_2 - \lambda_3)(\hat{\mathbf{e}}_1 \hat{\mathbf{e}}_1^T + \hat{\mathbf{e}}_2 \hat{\mathbf{e}}_2^T) \\ &\quad + \lambda_3(\hat{\mathbf{e}}_1 \hat{\mathbf{e}}_1^T + \hat{\mathbf{e}}_2 \hat{\mathbf{e}}_2^T + \hat{\mathbf{e}}_3 \hat{\mathbf{e}}_3^T) \\ &= (\lambda_1 - \lambda_2)\mathbf{D}_l + (\lambda_2 - \lambda_3)\mathbf{D}_p + \lambda_3 \mathbf{D}_s,\end{aligned}$$

where $(\lambda_1 - \lambda_2)$, $(\lambda_2 - \lambda_3)$ and λ_3 are the coordinates of $\mathbf{D}$ in the tensor basis $\{\mathbf{D}_l, \mathbf{D}_p, \mathbf{D}_s\}$. A similar tensor shape analysis has shown to be useful in a number of computer vision applications (Westin and Knutsson, 1992, 1994).

The coordinates of the tensor in our new basis classify the diffusion tensor and describe how close the tensor is to the generic cases of line, plane and sphere; and hence can be used for classification of the diffusion tensor according to its geometry. Since the coordinates are based on the eigenvalues of the tensor, they are rotationally invariant and the values do not depend on the chosen frame of reference. To obtain quantitive measures of the anisotropy, the derived coordinates have to be normalized, which, in turn, will lead to geometric shape measures. As in the case of fractional and relative anisotropy, there are several (rotationally invariant) choices of normalization. For example the maximum diffusity, λ_1, the trace of the tensor, $\lambda_1 + \lambda_2 + \lambda_3$, or the norm of the tensor, $(\lambda_1^2 + \lambda_2^2 + \lambda_3^2)^{1/2}$, can be used as normalization factors.

By using the largest eigenvalues of the tensor, the following quantitive shape measures are obtained for the linear, planar and spherical measures,

$$c_l = \frac{\lambda_1 - \lambda_2}{\lambda_1}, \tag{33}$$

$$c_p = \frac{\lambda_2 - \lambda_3}{\lambda_1}, \tag{34}$$

$$c_s = \frac{\lambda_3}{\lambda_1}, \tag{35}$$

where all measures lie in the range from zero to one, and their sum is equal to one,

$$c_l + c_p + c_s = 1. \tag{36}$$

Fig. 4 contains coronal brain images depicting these geometrical measures. Alternatively the coordinates can be normalized with the norm of the tensor giving

$$c_l = \frac{\lambda_1 - \lambda_2}{\sqrt{\lambda_1^2 + \lambda_2^2 + \lambda_3^2}}, \tag{37}$$

$$c_p = \frac{2(\lambda_2 - \lambda_3)}{\sqrt{\lambda_1^2 + \lambda_2^2 + \lambda_3^2}}, \tag{38}$$

$$c_s = \frac{3\lambda_3}{\sqrt{\lambda_1^2 + \lambda_2^2 + \lambda_3^2}}. \tag{39}$$

To ensure that the measures remain in the range from zero to one, and the sum is one, the scaling factors 2 and 3 have been inserted for the planar and the spherical case. A geometrical anisotropy measure that has a behavior similar to the FA measure (fractional anisotropy, Eq. (27)) is a measure describing the deviation from the spherical case,

$$c_a = 1 - c_s = c_l + c_p, \tag{40}$$

which is the sum of the linear and planar measure. By normalizing with the trace of the tensor instead of the norm, the measure will be more similar to the RA measure (relative anisotropy, Eq. (27)).

The presented measures quantitatively describe the geometrical shape of the diffusion tensor and therefore do not depend on the absolute level of the diffusion present. However, in low signal regions, where the noise level dominates these shape measures, they make little sense. In practice, all shape measures should be regularized by adding a constant in the denominator of size similar to that of the noise level. For example, the λ_1 normalized linear measure (Eq. (33)) would be expressed as follows:

$$c_{l_\sigma} = \frac{\lambda_1 - \lambda_2}{\lambda_1 + \sigma}, \tag{41}$$

where a suitable value for σ would be the expected value of λ_1 in a low signal region. This expression has similarities to classical Wiener filtering where the noise level σ has very little influence on signals larger than σ, but

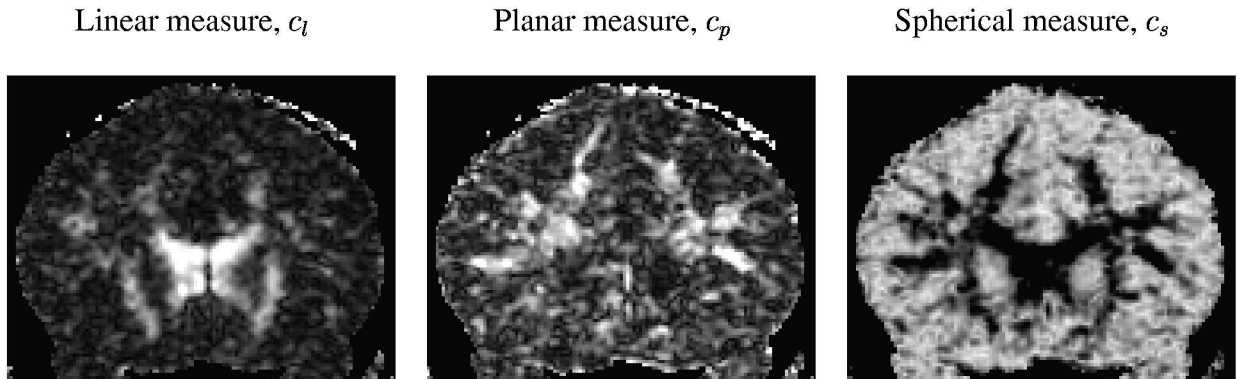Linear measure, c_l Planar measure, c_p Spherical measure, c_s

Fig. 4. Coronal brain images showing the three geometrical measures. Note that most of the major fiber tracts are visible despite the low resolution of the data set ($1.7 \times 1.7 \times 4$ mm).

penalizes signals that are smaller. When the normalization is done using the trace or norm, σ should have the expected value of the trace or norm respectively in low signal regions.

When applied to white matter, the linear measure, c_l, reflects the uniformity of tract direction within a voxel. In other words, it will be high only if the diffusion is restricted in two orthogonal directions. The anisotropy measure, c_a, indicates the relative restriction of the diffusion in the most restricted direction and will emphasize white matter tracts, which, within a voxel, will exhibit at least one direction of relatively restricted diffusion.

4.2. Macrostructural tensor and diffusive measures

In the previous section, we characterized the diffusion isotropy and anisotropy within a voxel. Here, we will discuss methods for examining the pattern or distribution of diffusion within a local image neighborhood. Basser and Pierpaoli proposed a scalar measure for macrostructural diffusive similarity based on tensor inner products between the center voxel tensor and its neighbors (Basser and Pierpaoli, 1996; Pierpaoli and Basser, 1996) (as in the vector case, the inner product between two tensors measures their degree of similarity). This intervoxel scalar measure is known as a 'lattice' index and is defined by[1]

$$LI = \sum_k a_k \left(\frac{\sqrt{3}}{\sqrt{8}} \frac{\sqrt{\langle \mathbf{T}, \mathbf{T}_k \rangle}}{\sqrt{\langle \mathbf{D}, \mathbf{D}_k \rangle}} + \frac{3}{4} \frac{\langle \mathbf{T}, \mathbf{T}_k \rangle}{\sqrt{\langle \mathbf{D}, \mathbf{D} \rangle}\sqrt{\langle \mathbf{D}_k, \mathbf{D}_k \rangle}} \right), \quad (42)$$

where a_k is a spatial mask, for example, 3×3 voxels, with sum of coefficients equal to one, and $\mathbf{T}$ is the anisotropic part of the diffusion tensor $\mathbf{D}$. The anisotropic part of the tensor has trace zero and can be written as

$$\mathbf{T} = \mathbf{D} - \tfrac{1}{3} \text{trace}(\mathbf{D})\mathbf{I}, \quad (43)$$

$$= \mathbf{D} - \tfrac{1}{3}\langle \mathbf{D}, \mathbf{I} \rangle, \quad (44)$$

$$= \mathbf{D} - \frac{\langle \mathbf{D}, \mathbf{I} \rangle}{\langle \mathbf{I}, \mathbf{I} \rangle}, \quad (45)$$

where $\mathbf{I}$ is the identity tensor. By rewriting Eq. (42) it becomes clear that all the tensor inner products are individually normalized,

$$LI = \sum_k a_k \left(\sqrt{\frac{3}{8}} \sqrt{\frac{\langle \mathbf{T}, \mathbf{T}_k \rangle}{\langle \mathbf{D}, \mathbf{D}_k \rangle}} + \frac{3}{4} \sqrt{\frac{\langle \mathbf{T}, \mathbf{T}_k \rangle}{\langle \mathbf{D}, \mathbf{D} \rangle}} \sqrt{\frac{\langle \mathbf{T}, \mathbf{T}_k \rangle}{\langle \mathbf{D}_k, \mathbf{D}_k \rangle}} \right). \quad (46)$$

Since the components in the sum are normalized, small and large diffusion tensor components will have equal weight in determining the lattice index. Unfortunately the smaller tensors are more influenced by noise and hence affect the index more than is desirable.

An alternative measure to the lattice index, which can be

seen as an external measure since it is based on the tensors in a neighborhood, is to use an internal voxel based measure (RA, FA, $c_{l,p,s}$) on a *filtered* version of the diffusion tensor field. For example, local averaging of the tensor field with a spatial mask a (normalized so the coefficients sum to one),

$$\mathbf{D}_a = \sum_k a_k \mathbf{D}_k, \quad (47)$$

describes the local average diffusion where the rank of the average tensor $\mathbf{D}_a$ describes the complexity of the macroscopic diffusion structure. If the rank is close to one, the structure is highly linear, which will be the case in regions of bundles of fibers having the same direction. If the rank is two, fibers are crossing in a plane, or the underlying diffusivity is planar. Applying the above geometrical linear measure, c_l (Eq. (33)), to this tensor gives a measure that is high in regions with coherent tensors.

Fig. 5 compares the three original geometrical measures (top) and the same measures applied to the same tensor data averaged by a Gaussian mask (bottom). Major white matter tracts such as the corpus callosum show high linearity in the averaged data set, indicating high macrostructural organization. It should be noted that averaging of a diffusion tensor field and then deriving a scalar measure from the averaged field is not the same as averaging the scalar measure derived from the original field.

The relatively simple approach of averaging is useful because the rank of the the tensors increases when lower rank, non-collinear tensors are summed. This effect is illustrated in Fig. 6 and compared to adding vectors which does not have the freedom to change rank. Adding the two vectors (a) and (b) results in a new vector (c), which is of the same order of complexity as the original vectors. However, adding two rank 1 tensors (d) and (e), e.g. diffusion tensors from two differently oriented white matter tracts, results in a rank 2 tensor (f), i.e. the output has more degrees of freedom than the input tensors and describes the plane in which diffusion is present. In this sense, averaging of tensors is different from averaging a vector field. The average of a set of vectors gives the 'mean event', while the average of a set of tensors gives the 'mean event' and the 'range of the present events'.

Fig. 7 shows a 2D example illustrating the effect of Gaussian filtering of a diffusion tensor field. The filtered areas that contain inconsistent data give a result of almost round ellipses (upper right half of the image). Moreover, Gaussian filtering results in more stable estimates of the field directionality in the areas where there is a clear bias in one direction (lower left).

The macrostructural measure achieved (by averaging the tensor field using an isotropic mask) is essentially a feature extraction method rather than a restoration method, where the latter aims at reducing the noise level in the data. Although our method does remove noise, the incorporation of more advanced regularization methods (Poupon et al.,

---

[1] Corrected formula, Pierpaoli, personal communication, 1997.

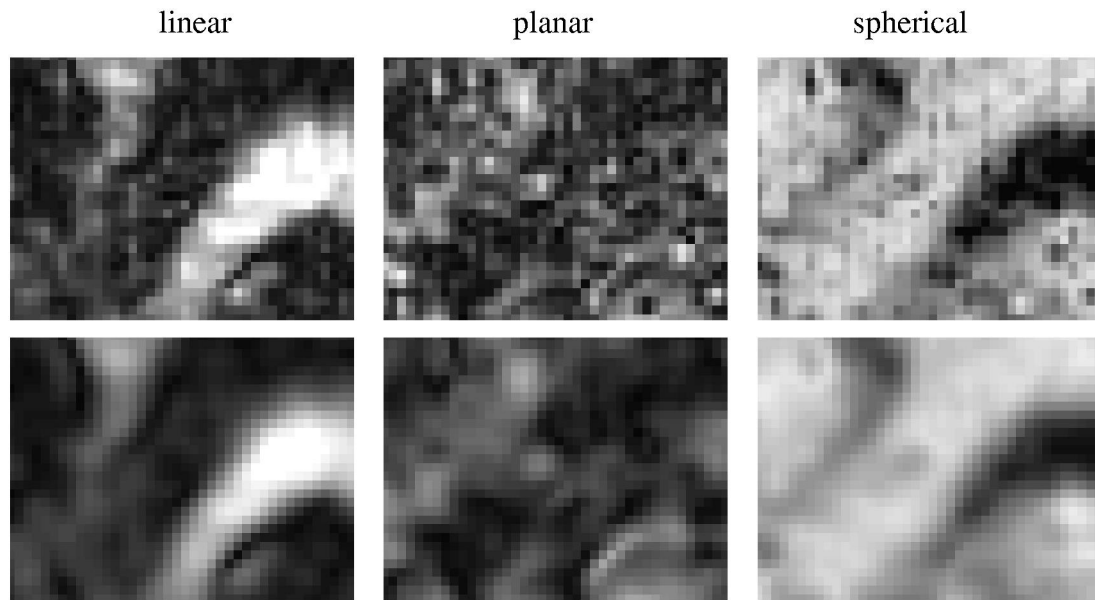linear   planar   spherical

Fig. 5. Axial brain images showing the three geometrical measures and corresponding macrostructural diffusion measures. Top: shows the geometrical measures derived from the original data. Bottom: shows the corresponding macrostructural diffusion measures: the geometrical measures derived from the tensors averaged with a $9\times9\times3$ Gaussian kernel.

2000; Parker et al., 2000) should be explored, if noise reduction is the main target. Anisotropic filter masks are preferable since they reduce the risk of blurring edges. However, using an anisotropic mask for the macrostructur-al measure would limit its purpose, the description of the organization within an area. If the signal is changing due to edges inside the local area of interest, this should be reflected in the measure.
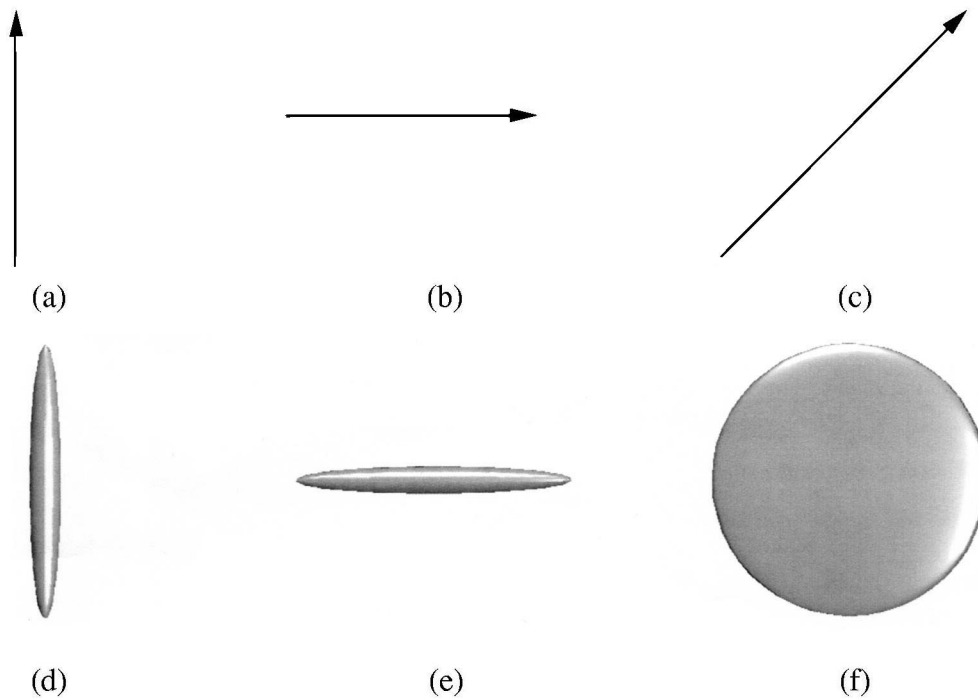

Fig. 6. Vector and tensor summation. Two vectors, (a) and (b), and their sum (c). Two diffusion tensors, (d) and (e), of rank close to 1 visualized as ellipsoids with eigenvectors forming principal axes. The summation of the two tensors gives a rank 2 tensor (f).
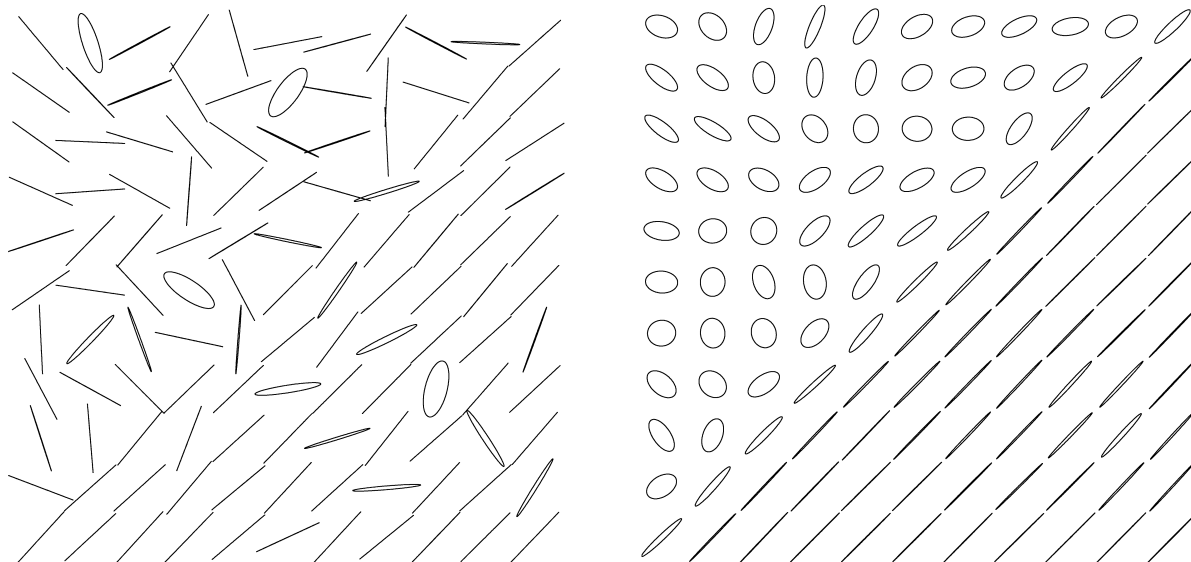
Fig. 7. A 2D diffusion tensor field (left) and the effect of relaxation using a Gaussian filter (right). Note how the tensors in an inconsistent region become rounder, whereas in consistent areas their orientation is stabilized.

5. Visualization of diffusion tensors

Several methods have been proposed for visualizing the information contained in DT-MRI data. Pierpaoli et al. (1996) renders ellipsoids to visualize diffusion data in a slice. Peled et al. (1998) used headless arrows to represent the in-plane component of the principal eigenvector, along with a color coded out-of-plane component. Recently, Kindlmann and Weinstein (1999) applied our geometric shape indicies (Westin et al., 1997) to opacity maps in volume rendering. They termed this method 'barycentric opacity mapping'. They compare volume renderings using opacity maps based on the indices c_l, c_p and c_a (Eqs. (37)–(40)).

In Fig. 8 (left) a diffusion tensor field from an axial slice of the brain is shown (using the visualization method presented in Peled et al., 1998) and the filtered tensor field (right). Prior to visualization, the tensors have been weighted with their linear diffusion measure.

The filtered images shows the result of applying the macrostructural measure presented in Section 4.2. First a $5 \times 5 \times 3$ Gaussian window, a, with standard deviation

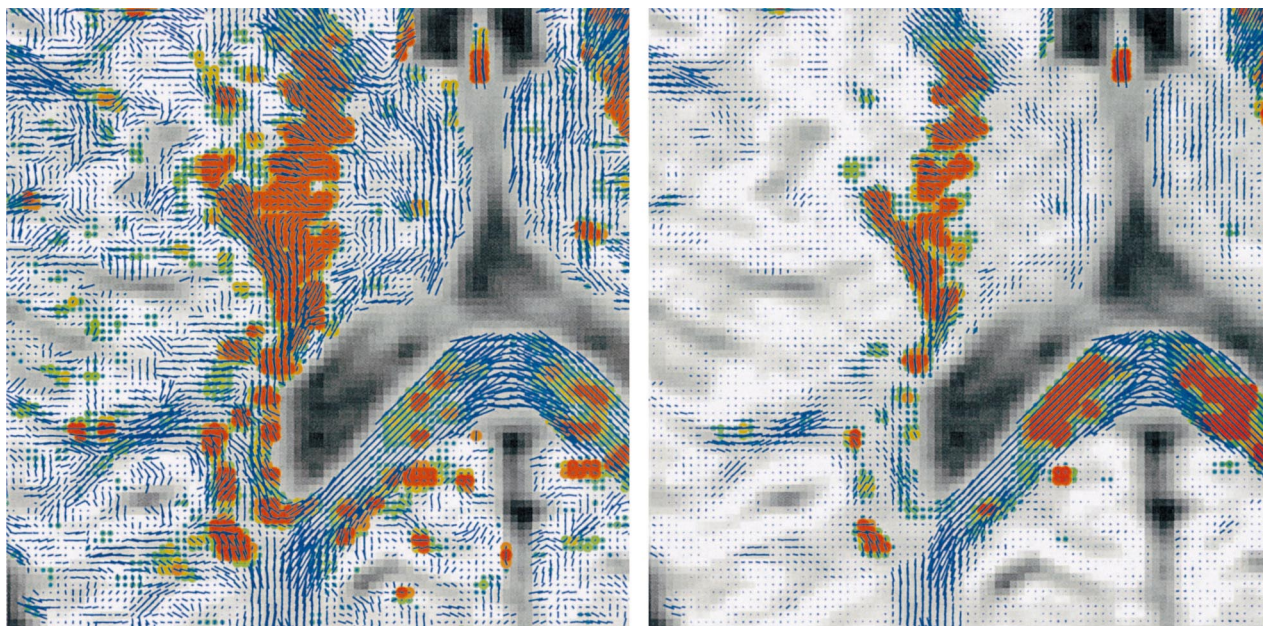
Fig. 8. Left: Diffusion tensors, weighted with their linear measure c_l, from an axial slice of a human brain. Right: Averaged diffusion tensors using a $5 \times 5 \times 3$ Gaussian kernel weighted with their linear measure c_l, resulting in a macrostructural measure of fiber tract organization.
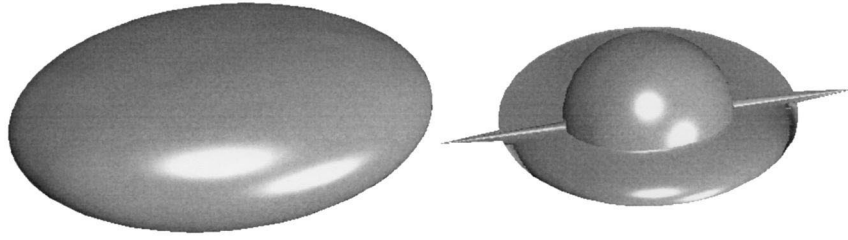
Fig. 9. Comparison of an ellipsoid and a composite shape depicting the same tensor with eigenvalues $\lambda_1 = 1$, $\lambda_2 = 0.7$ and $\lambda_3 = 0.4$.

equal to 2 mm was applied to the data (Eq. (47)). Since the out-of-plane resolution is slightly less than half the in-plane resolution, there is almost no smoothing performed between the slices. The tensors resulting from the Gaussian filtering $\mathbf{D}_a$ (Eq. (47)) have been weighted with their linear diffusion measure, c_l (Eq. (37)), respectively. The result illustrates the fact that the filtering increases the rank of the tensors in non-structured areas since the linear measures are decreased in those areas.

As mentioned above, in 3D, a diffusion tensor can be visualized using an ellipsoid where the principal axes correspond to the tensor's eigenvector system. However, it is difficult to distinguish between an edge-on, flat ellipsoid and an oblong one using the surface shading information. Similar ambiguity exists between a face-on, flat ellipsoid and a sphere. We propose a technique for the visualization of tensor fields that overcomes the problems with ellipsoids. Fig. 9 compares the ellipsoidal representation of a tensor (left) with a composite shape of linear, planar and spherical components (right). The components are here scaled according to the eigenvalues, but can alternatively be scaled according to the shape measures c_l, c_p and c_s.

Additionally, coloring based on the shape measures c_l, c_p and c_s can be used for visualization of shape. Fig. 10 shows a coloring scheme where the color is interpolated between the blue linear case, the yellow planar case and the red spherical case.

6. White matter tractography

DT-MRI provides a unique tool for investigating brain structures and for assessing axonal fiber connectivity in vivo. Recent work includes (Conturo et al., 1999; Jones et al., 1999; Poupon et al., 2000; Basser et al., 2000). In this section we will expand on the tractography method presented in (Westin et al., 1999) and present some novel results.

The algorithm for tracing co-linear diffusion tensors is based on using the diffusion tensors as projection operators. Let $\mathbf{x}_0$ be the initial seed point, and $\mathbf{v}_0$ be the seed direction, e.g. the eigenvector corresponding to the largest eigenvalue. A tracing sequence $\{\mathbf{x}_0, \mathbf{x}_1, \ldots\}$ can then be obtained by the following iteration formula:

$$\mathbf{x}_{k+1} = \mathbf{x}_k + \alpha \hat{\mathbf{v}}_k, \tag{48}$$

$$\mathbf{D}_{k+1} = F(\mathbf{D}(\mathbf{x}_{k+1})), \tag{49}$$

$$\mathbf{v}_{k+1} = \mathbf{D}_{k+1} \mathbf{v}_k, \tag{50}$$

where $\mathbf{D}(\mathbf{x}_{k+1})$ is the tensor in spatial position $\mathbf{x}_{k+1}$ (interpolated from the tensor field $\mathbf{D}$) and F is a function that maps the eigenvalues,

$$F(\mathbf{D}) = \sum_{k=1}^{3} f_k(\lambda_k) \hat{\mathbf{e}}_k \hat{\mathbf{e}}_k^{\mathrm{T}}, \tag{51}$$

where f_k are scalar functions. Since the effect of the function F is only a weighting of the original tensor basis functions $\hat{\mathbf{e}}_k \hat{\mathbf{e}}_k^{\mathrm{T}}$, only the eigenvalues of the tensor are changed, and not its eigenvector system. The functions f_k can, for example, serve as thresholding operators, which, in turn, results in decreased tensor rank when the eigenvalues are smaller than a specified threshold.

When the tensor $\mathbf{D}_{k+1}$ in Eq. (50) is anisotropic, the result of the operation $\mathbf{D}_{k+1} v_k$ is a vector v_{k+1} which is turned towards the largest eigenvector of the tensor relative to the vector v_k. However, the direction of this vector will not coincide with the principal axis of the diffusion ellipsoid, since a bias will be introduced by the contributions from the projections on the other two eigenvectors of $\mathbf{D}_{k+1}$.

One possible remedy to this is to use a function F that sets the two smaller eigenvalues to zero ($\lambda_2 = \lambda_3 = 0$) creating a projection operator that projects any vector onto the orientation of the principal eigenvector, $\mathbf{e}_1$,

$$F_{\lambda_1}(\mathbf{D}) = \lambda_1 \mathbf{e}_1 \mathbf{e}_1^{\mathrm{T}}. \tag{52}$$

With this function, the iteration formula above becomes equivalent to following the direction of the principal eigenvector. The ambiguity whether to step in the direction $\mathbf{e}_1$ or $-\mathbf{e}_1$ is avoided in this projection operator formulation.

Unfortunately, the strategy to follow the principal direction is inherently unstable. The main reason is that if $\lambda_1 = \lambda_2$, the direction of $\mathbf{e}_1$ is only defined up to a plane, but not which direction in the plane. Fig. 11 illustrates this problem in a 2D example. Collinear tensors with varying degrees of isotropy, with maximum isotropy in the middle
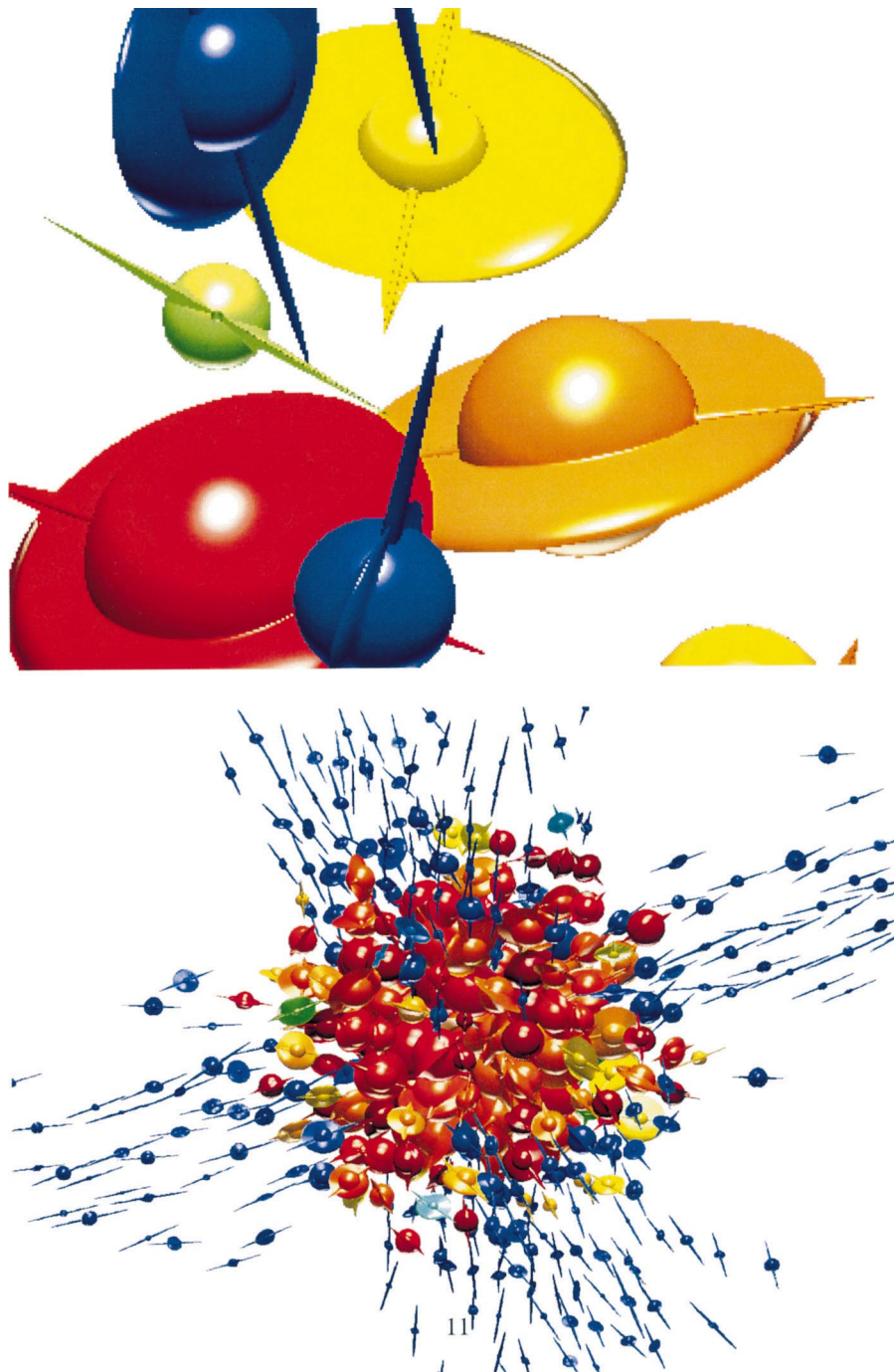
Fig. 10. Visualization of diffusion tensors. The tensors are color coded according to the shape: linear case is blue, planar case is yellow, and spherical case is red. The radius of the sphere is the smallest eigenvalue of the diffusion tensor; the radius of the disk is second largest; and the length of the rod is twice the largest eigenvalue. The right image shows a simulated tensor field of three crossing white matter tracts. Due to partial voluming effects, the tensors in the area where the fibers are crossing have spherical shape.

where $\lambda_1 = \lambda_2$, are shown (Fig. 11(a)). The line inside the ellipses shows the direction of the principal eigenvector. For the middle ellipses, all directions are potential eigenvectors, and thus the calculated direction depends only on the eigenvalue algorithm at hand, and not the data. Using Matlab from Mathworks to calculate the eigenvector results in a vertical vector (Fig. 11(a)). In 3D, the same ambiguity arises when the tensor is spherical, since all

vectors are eigenvectors. Adding a noise component (Fig. 11(b)) introduces not only small biases on the directions of the eigenvectors, but introduces sorting errors, making the previously minor axis becoming the major axis of the ellipse.

Since the direction of the eigenvector corresponding to the largest eigenvalue is very unstable when in proximity to the generic cases of planar and spherical diffusion, an
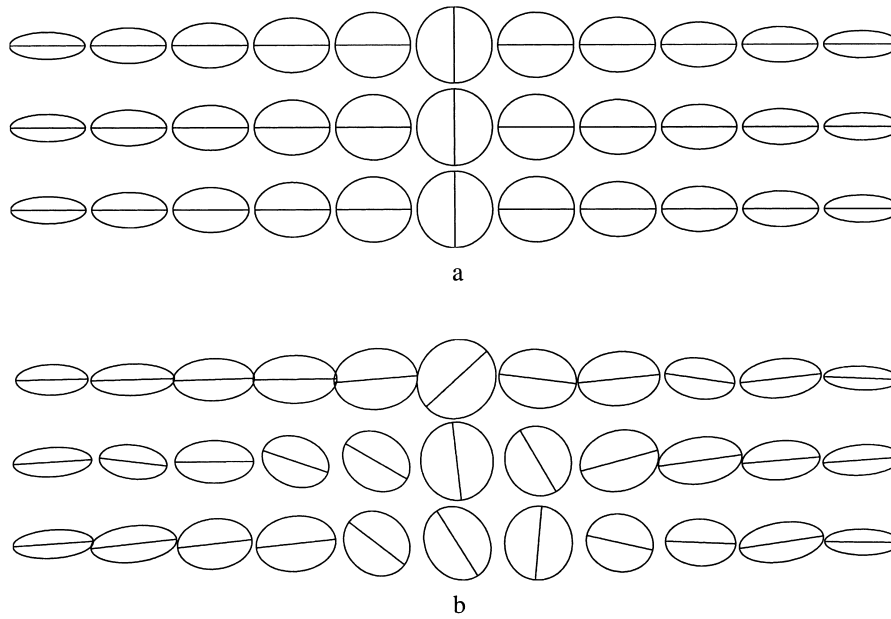
a

b

Fig. 11. Collinear diffusion tensor.

alternative is to map the eigenvalues of the tensor so the resulting tensor belongs to one of the generic cases of line, plane, or sphere, or at least make it closer to those cases. An example of this is to use the shape coordinates,

$$\mathbf{D} = \begin{cases} c_l \mathbf{D}_l, & \text{if } c_l > c_p, c_s, \\ c_p \mathbf{D}_p, & \text{if } c_p > c_l, c_s, \\ c_s \mathbf{D}_s, & \text{if } c_s > c_l, c_p. \end{cases} \qquad (53)$$

This operation forces the tensor into the closest of the three generic shapes: line, plane and sphere. For example, when the tensor is almost spherical, the mapped tensor $\mathbf{D}_{k+1}$ in Eq. (50) then will become the identity matrix (the tensor ellipsoid is a sphere), and the result of the operation $\mathbf{D}_{k+1} v_k$ (Eq. (50)) is v_k, i.e., the output vector $v_{k+1} = v_k$. In our experiments, we have used the mapping in Eq. (53). Although the tracing results are very promising, clearly, the question of how to best map the eigenvalues should be investigated further.

Fig. 12 shows the result of tracing three crossing fiber tracts. A $5 \times 5 \times 5$ Gaussian operator was used to define the macroscopic organization. Each trace line is composed of the combined results from both seed directions $\mathbf{e}_1$ and $-\mathbf{e}_1$.

Fig. 13 shows the result of three-dimensional tractography of a normal subject showing the anterior (yellow) and posterior (blue) part of the corpus callosum as well as the left and right (red and green) cortico-spinal tract. The tracts pass through an axial section of the later ventricles. The path was computed using the 'max-shape' mapping function (Eq. (53)) in the iteration formula (Eq. (48)). The seeds for the tractography were automatically determined by applying a connectivity algorithm on the linear measure c_l above a threshold. The connectivity was calculated in

the axial slice shown in Fig. 13. The four largest connected components were chosen, and different colors (red, blue, yellow and green) were assigned to the seeds.

7. Conclusions

We have proposed measures classifying diffusion tensors into three generic cases based on a tensor basis expansion. When applied to white matter, the linear index shows uniformity of tract direction within a voxel, while the anisotropic index quantifies the deviation from spatial homogeneity. The non-orthogonal tensor basis chosen is intuitively appealing since it is based on three simple, yet descriptive, geometrically meaningful cases.

We have presented a new method for calculating the diffusion tensors from the diffusion gradient raw data. The method is based on an analytic solution of the Stejskal– Tanner formula eliminating the need to solve the Stejskal– Tanner equation system for each voxel of the data set. We have also described how tensor diffusion data can be processed without reverting to the use of only scalar measures of the tensor data. By staying in the tensor domain, macroscopical features can be derived using relatively simple methods such as averaging the tensor field and classifying the change of diffusion geometry. We discussed the geometric addition of tensors and argued that adding tensors and vectors differ in that tensor summation gives more than the 'mean' event due to more degrees of freedom. By using the geometric diffusion measures on locally averaged tensors, local directionality consistency can be determined (e.g. existence of larger fiber tracts). We are confident this averaging approach can be used to derive a tensor field that describes macrostructural features in the
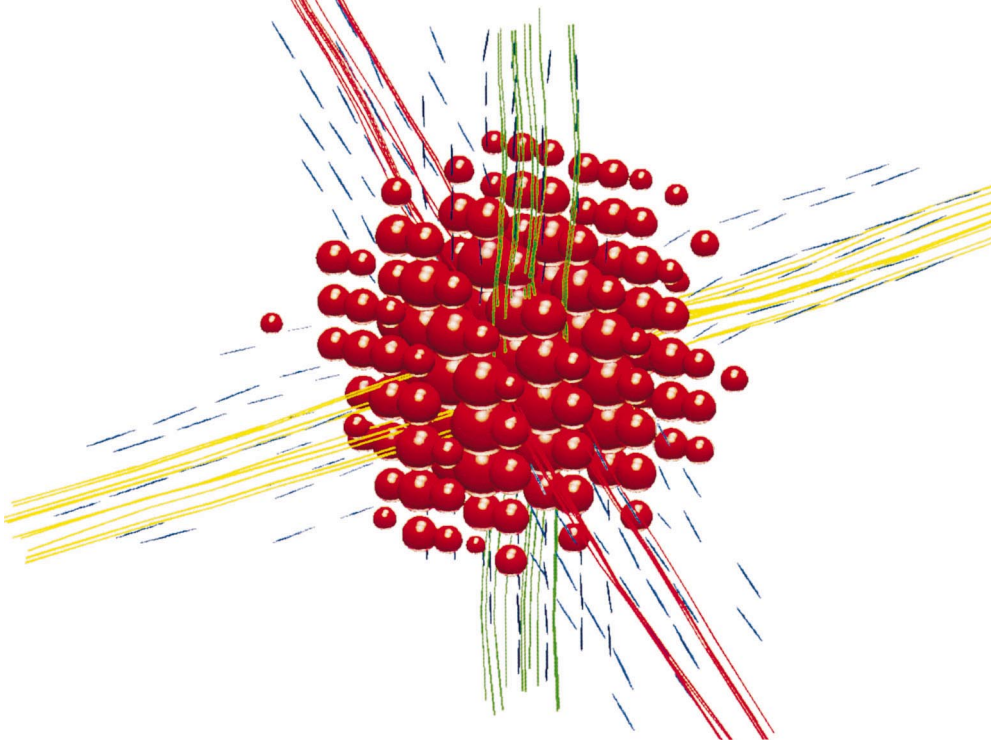
Fig. 12. The image shows the result of automatic tracing of collinear tensors in the 'three crossing tracts' data above (trace line in red, yellow and green). The data was first filtered with a $5\times5\times5$ Gaussian operator to remove noise, followed by the 'max shape' operator to facilitate the tracking. Ten points were randomly seeded at one end of each of the three branches. Note how the stream lines 'tunnel' through the area in the center where the information of directionality is uncertain.

tensor diffusion data. The linear measure c_l derived from the averaged tensor field can, for example, be used for quantitative evaluation of fiber tract organization. One limitation with this method is that if a large mask is chosen, information about medium to small fiber bundles will be lost. Care has to be taken when choosing the mask. We also have described how mapped diffusion tensors can be used for tracing white matter tracts in the human brain. The mapping alleviates the need to blindly follow the direction of maximum diffusion which is inherently unstable in regions of planar or spherical tensors.

Acknowledgements

Appendix A

In Section 3.1 we derived a compact solution to the Stejskal–Tanner equation system (Eq. (6)) using concepts from tensor analysis, and presented explicit numbers for our specific gradient configuration. In this section, the result from using the gradient configuration in (Basser and Pierpaoli, 1996) is presented. These gradients are

$$\mathbf{g}_1 = \frac{1}{\sqrt{2}}\begin{pmatrix} 1 \\ 0 \\ -1 \end{pmatrix}, \quad \mathbf{g}_2 = \frac{1}{\sqrt{2}}\begin{pmatrix} -1 \\ 0 \\ 1 \end{pmatrix}, \quad \mathbf{g}_3 = \frac{1}{\sqrt{2}}\begin{pmatrix} 0 \\ 1 \\ 1 \end{pmatrix},$$

$$\mathbf{g}_4 = \frac{1}{\sqrt{2}}\begin{pmatrix} 0 \\ 1 \\ -1 \end{pmatrix}, \quad \mathbf{g}_5 = \frac{1}{\sqrt{2}}\begin{pmatrix} 1 \\ 1 \\ 0 \end{pmatrix}, \quad \mathbf{g}_6 = \frac{1}{\sqrt{2}}\begin{pmatrix} -1 \\ 1 \\ 0 \end{pmatrix},$$

$$(A.1)$$

giving the following outer products of these gradients:

$$\mathbf{G}_1 = \frac{1}{2}\begin{pmatrix} 1 & 0 & 1 \\ 0 & 0 & 0 \\ 1 & 0 & 1 \end{pmatrix}, \quad \mathbf{G}_2 = \frac{1}{2}\begin{pmatrix} 1 & 0 & -1 \\ 0 & 0 & 0 \\ -1 & 0 & 1 \end{pmatrix},$$

$$\mathbf{G}_3 = \frac{1}{2}\begin{pmatrix} 0 & 0 & 0 \\ 0 & 1 & 1 \\ 0 & 1 & 1 \end{pmatrix}, \quad (A.2)$$

$$\mathbf{G}_4 = \frac{1}{2}\begin{pmatrix} 0 & 0 & 0 \\ 0 & 1 & -1 \\ 0 & -1 & 1 \end{pmatrix},$$

$$\mathbf{G}_5 = \frac{1}{2}\begin{pmatrix} 1 & 1 & 0 \\ 1 & 1 & 0 \\ 0 & 0 & 0 \end{pmatrix}, \quad \mathbf{G}_6 = \frac{1}{2}\begin{pmatrix} 1 & -1 & 0 \\ -1 & 1 & 0 \\ 0 & 0 & 0 \end{pmatrix}. \quad (A.3)$$

A convenient way of finding the dual basis is by stacking the coordinates of each basis element as a column vector in a matrix, and calculating the pseudo inverse of this matrix $\tilde{\mathbf{G}} = \mathbf{G}^{\dagger}$,
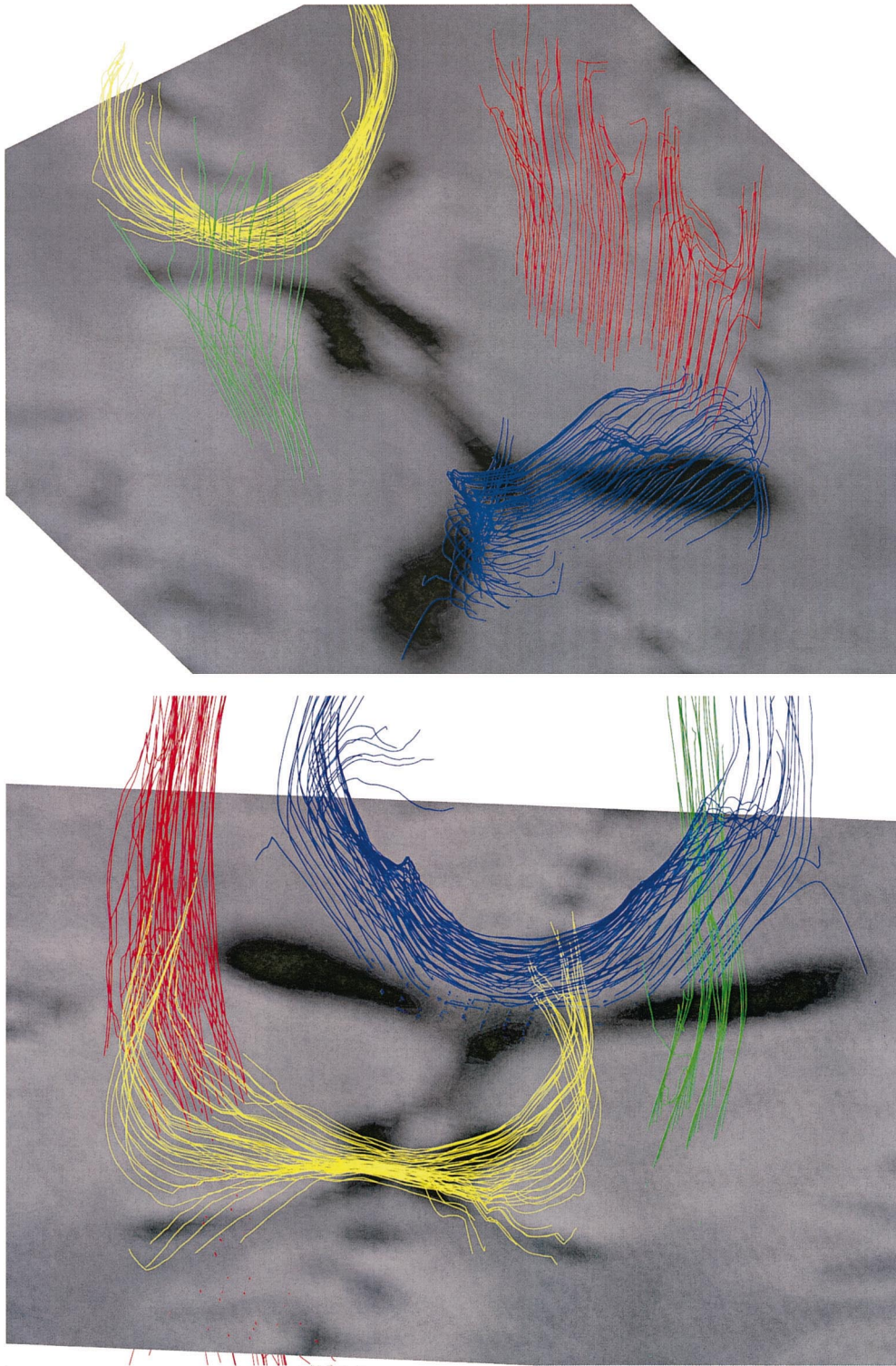
Fig. 13. Three-dimensional tractography of a normal subject showing the anterior (yellow) and posterior (blue) part of the corpus callosum as well as the left and right (green and red) cortico-spinal tract. The tracts pass through an axial section of the later ventricles. Top and bottom images present two different views of the tractography result.

$$
\begin{pmatrix} | & | & \cdots & | \\ \mathbf{G}_1 & \mathbf{G}_2 & \cdots & \mathbf{G}_6 \\ | & | & \cdots & | \end{pmatrix}^{\dagger}
$$

$$
= \left(\frac{1}{2} \begin{pmatrix} 1 & 1 & 0 & 0 & 1 & 1 \\ 0 & 0 & 0 & 0 & 1 & -1 \\ 1 & -1 & 0 & 0 & 0 & 0 \\ 0 & 0 & 0 & 0 & 1 & -1 \\ 0 & 0 & 1 & 1 & 1 & 1 \\ 0 & 0 & 1 & -1 & 0 & 0 \\ 1 & -1 & 0 & 0 & 0 & 0 \\ 0 & 0 & 1 & -1 & 0 & 0 \\ 1 & 1 & 1 & 1 & 0 & 0 \end{pmatrix} \right)^{\dagger} \tag{A.4}
$$

$$
= \frac{1}{2} \begin{pmatrix} 1 & 0 & 1 & 0 & -1 & 0 & 1 & 0 & 1 \\ 1 & 0 & -1 & 0 & -1 & 0 & -1 & 0 & 1 \\ -1 & 0 & 0 & 0 & 1 & 1 & 0 & 1 & 1 \\ -1 & 0 & 0 & 0 & 1 & -1 & 0 & -1 & 1 \\ 1 & 1 & 0 & 1 & 1 & 0 & 0 & 0 & -1 \\ 1 & -1 & 0 & -1 & 1 & 0 & 0 & 0 & -1 \end{pmatrix}. \tag{A.5}
$$

The rows of the pseudo inverse (Eq. (A.5)) contain the dual basis elements. Reshaping them into 3×3 tensors gives

$$
\tilde{\mathbf{G}}_1 = \frac{1}{2} \begin{pmatrix} 1 & 0 & 1 \\ 0 & -1 & 0 \\ 1 & 0 & 1 \end{pmatrix}, \quad \tilde{\mathbf{G}}_2 = \frac{1}{2} \begin{pmatrix} 1 & 0 & -1 \\ 0 & -1 & 0 \\ -1 & 0 & 1 \end{pmatrix},
$$

$$
\tilde{\mathbf{G}}_3 = \frac{1}{2} \begin{pmatrix} -1 & 0 & 0 \\ 0 & 1 & 1 \\ 0 & 1 & 1 \end{pmatrix}, \quad \tilde{\mathbf{G}}_4 = \frac{1}{2} \begin{pmatrix} -1 & 0 & 0 \\ 0 & 1 & -1 \\ 0 & -1 & 1 \end{pmatrix},
$$

$$
\tilde{\mathbf{G}}_5 = \frac{1}{2} \begin{pmatrix} 1 & 1 & 0 \\ 1 & 1 & 0 \\ 0 & 0 & -1 \end{pmatrix}, \quad \tilde{\mathbf{G}}_6 = \frac{1}{2} \begin{pmatrix} 1 & -1 & 0 \\ -1 & 1 & 0 \\ 0 & 0 & -1 \end{pmatrix}.
$$

References

Basser, P., 1995. Inferring microstructural features and the physiological state of tissues from diffusion-weighted images. NMR Biomed. 8, 333–344.

Basser, P., Pierpaoli, C., 1996. Microstructural and physiological features of tissues elucidated by quantitative-diffusion-tensor MRI. J. Magn. Reson. Ser. B 111, 209–219.

Basser, P., Pajevic, S., Pierpaoli, C., Duda, J., Aldroubi, A., 2000. In vivo fiber tractography using DT-MRI data. Magn. Reson. Med. 44, 625–632.

Beaulieu, C., Allen, P., 1994. Determinants of anisotropic water diffusion in nerves. Magn. Reson. Med. 31, 394–400.

Chenevert, T., Brunberg, J., Pipe, J., 1990. Anisotropic diffusion in human white matter: demonstration with MR techniques in vivo. Radiology 177, 401–405.

Conturo, T.E., Lori, N.F., Cull, T.S., Akbuda, E., Snyder, A.Z., Shimony, J.S., McKinstry, R.C., Burton, H., Raichle, A.E., 1999. Tracking neuronal fiber pathways in the living human brain. Neurobiology 96, 10422–10427.

Einstein, A., 1905. Über die von der molekularkinetischen theorie der wärme geforderte bewegung von in ruhenden flüssigkeiten suspendierten teilchen. Ann. Phys. 17, 549–560.

Fick, A., 1855. Über diffusion. Ann. Phys., 94–99.

Fourier, J., 1822. Théorie analytique de la chaleur. Académie des Sciences.

Gudbjartsson, H., Maier, S., Mulkern, R., Mórocz, I.A., Patz, S., Jolesz,

F., 1996. Line scan diffusion imaging. Magn. Reson. Med. 36, 509–519.

Jones, D.K., Simmons, A., Williams, S.C.R., Horsfield, M.A., 1999. Non-invasive assessment of axonal fiber connectivity in the human brain via diffusion tensor MRI. Magn. Reson. Med. 42, 37–41.

Kendall, D.E.B.P., 1977. Vector Analysis and Cartesian Tensors. Van Nostrand Reinhold, UK.

Kindlmann, G., Weinstein, D., 1999. Hue balls and lit-tensors for direct volume rendering of diffusion tensor fields. In: IEEE Visualization 1999, VIS1999, Salt Lake City, UT.

LeBihan, D., Breton, E., Lallemand, D., Grenier, P., Cabanis, E., Laval-Jeantet, M., 1986. MR imaging of intravoxel incoherent motions: application to diffusion and perfusion in neurologic disorders. Radiology 161, 401–407.

Maier, S., Gudbjartsson, H., 1998. Line scan diffusion imaging. USA patent #5,786692.

Maier, S., Gudbjartsson, H., Patz, S., Hsu, L., Lovblad, K.-O., Edelman, R., Warach, S., Jolesz, F., 1998. Line scan diffusion imaging: characterization in healthy patients and stroke patients. Am. J. Roentgenol. 17 (1), 85–93.

Moseley, M.E., Cohen, Y., Kucharczyk, J., Mintorovitch, J., Asgari, H.S., Wendland, M.F., Tsuruda, J., Norman, D., 1990. Diffusion-weighted MR imaging of anisotropic water diffusion in the central nervous system. Radiology 176, 439–445.

Parker, G.J.M., Schnabel, J.A., Symms, M.R., Werring, D.J., Barker, G.J., 2000. Nonlinear smoothing for reduction of systematic and random errors in diffusion tensor imaging. J. Magn. Reson. Imaging 11, 702–710.

Peled, S., Gudbjartsson, H., Westin, C.-F., Kikinis, R., Jolesz, F., 1998. Magnetic resonance imaging shows orientation and asymmetry of white matter tracts. Brain Res. 780 (1), 27–33.

Pierpaoli, C., Basser, P.J., 1996. Toward a quantitative assessment of diffusion anisotropy. Magn. Reson. Med. 36, 893–906.

Pierpaoli, C., Jezzard, P., Basser, P.J., Barnett, A., Chiro, G.D., 1996. Diffusion tensor MR imaging of the human brain. Radiology 201, 637.

Poupon, C., Clark, C.A., Frouin, F., Régis, J., Bloch, I., Bihan, D.L., Bloch, I., Mangin, J.-F., 2000. Regularization of diffusion-based direction maps for the tracking of brain white matter fascicles. NeuroImage 12, 184–195.

Stejskal, E.O., Tanner, J.E., 1965. Spin diffusion measurements: spin echoes in the presence of a time-dependent field gradient. J. Chem. Phys. 42, 288–292.

Stoker, J.J., 1989. Differential Geometry. Wiley, New York.

Turner, R., le Bihan, D., Maier, J., Vavrek, R., Hedges, L.K., Pekar, J., 1990. Echo planar imaging of intravoxel incoherent motions. Radiology 177, 407–414.

Westin, C.-F., 1994. A tensor framework for multidimensional signal processing. Ph.D. thesis, Linköping University, Sweden (dissertation No. 348).

Westin, C.-F., Knutsson, H., 1992. Extraction of local symmetries using tensor field filtering. In: Proceedings of the 2nd Singapore International Conference on Image Processing. IEEE, Singapore.

Westin, C.-F., Knutsson, H., 1994. Estimation of motion vector fields using tensor field filtering. In: Proceedings of IEEE International Conference on Image Processing. IEEE, Austin, TX, pp. 237–242.

Westin, C.-F., Maier, S., Khidhir, B., Everett, P., Jolesz, F., Kikinis, R., 1999. Image processing for diffusion tensor magnetic resonance imaging. In: Medical Image Computing and Computer-Assisted Intervention. Lecture Notes in Computer Science, pp. 441–452.

Westin, C.-F., Peled, S., Gudbjartsson, H., Kikinis, R., Jolesz, F., 1997. Geometrical diffusion measures for MRI from tensor basis analysis. In: ISMRM '97, Vancouver, Canada, p. 1742.

Wimberger, D.M., Roberts, T.P., Barkovich, A.J., Prayer, L.M., Moseley, M.E., Kucharczyk, J., 1995. Identification of 'premyelination' by diffusion-weighted MRI. J. Comp. Assist. Tomogr. 19 (1), 28–33.

Young, E.C., 1978. Vector and Tensor Analysis. Dekker.